Journal of
Applied Crystallography
ISSN 0021-8898

Received 1 January 2002
Accepted 15 December 2006

Small-angle X-ray study of the three-dimensional collagen/mineral superstructure in intramuscular fish bone

Hongwen Zhou,[a] Christian Burger,[a] Igors Sics,[a] Benjamin S. Hsiao,[a] Benjamin Chu,[a]* Lila Graham[b] and Melvin J. Glimcher[b]

[a]Department of Chemistry, Stony Brook University, Stony Brook, NY 11794-3400, USA, and [b]Department of Orthopedic Surgery, Children's Hospital, Harvard Medical School, Boston, MA 02215, USA. Correspondence e-mail: bchu@notes.cc.sunysb.edu

Synchrotron small-angle X-ray scattering (SAXS) was conducted on native intramuscular shad/herring bone samples. Two-dimensional SAXS patterns were quantitatively analyzed with special consideration for preferred orientation effects, leading to new insights into the three-dimensional superstructure of mineralized collagen fibrils in shad/herring bone.

1. Introduction

The superstructure of bone has been extensively studied by electron microscopy, X-ray and neutron diffraction, *etc*. for many decades (for a review, see, *e.g.*, Glimcher, 1998). It is known that, despite large diversities in size, shape, and hierarchical structures, all mature bone is built from mineralized collagen fibrils. From a structural point of view, the mineralized fibril can be considered as a two-phase composite material, consisting of a pre-deposited organic scaffold impregnated with the mineral phase. The organic matrix is formed by a staggered arrangement of collagen molecules (Hodge & Petruska, 1963), leaving gaps between subsequent molecules in the molecule axis direction which leads to a characteristic alternating gap/overlap band pattern in the fibril axis direction. The mineral phase is in the form of nanometre-scale apatite platelets (Robinson, 1952; Kim *et al.*, 1995). Transmission electron microscopy (TEM) studies on newly formed bone tissues showed that the mineral crystals are initially deposited into the gap regions of the organic matrix, with their crystallographic *c* axes (of the hexagonal apatite unit cell) preferentially oriented about the fibril axis (Jackson, 1957; Lee & Glimcher, 1991).

The existing models for the collagen/mineral superstructure (see the review by Glimcher, 1998), however, only address the axial relationship between mineral and collagen. The lateral arrangement of the mineral crystals in the collagen matrix remains unclear. Electron microscopic tomography and image reconstruction were used to visualize the mineral crystals and the organic matrix in three-dimensional (3D) space (Landis *et al.*, 1993). However, the resolution (~4–6 nm) of this technique is limited and only lightly mineralized tissue can be studied. For heavily mineralized tissue sections, individual crystals are densely packed in the organic matrix and cannot be resolved by this technique. Small-angle X-ray scattering (SAXS) was used to investigate the lateral packing of the mineral phase in the organic scaffold by analyzing the near-equatorial diffuse scattering features in two-dimensional (2D) patterns from calcified tissue (Fratzl *et al.*, 1993; Fratzl, 1994). The model developed by those authors assumes that mineral crystals have irregular shape and are randomly distributed in the fibril cross section, which is inconsistent with the TEM observations (Kim *et al.*, 1995; Lee & Glimcher, 1991).

In the present work, the characteristic 'butterfly' pattern, originating from the apatite platelets and their lateral arrangement, was analyzed in terms of disordered lamellar stacks of platelet-shaped mineral crystals with intercalated organic layers consisting of a few collagen molecules, under the approximation of independent stacking statistics (Zernike & Prins, 1927). With the stack normals preferentially oriented perpendicular to the fibril axis, preferred orientation effects were quantitatively taken into account (Ruland & Tompa, 1968; Burger *et al.*, 2007*a*). This analysis leads to thickness distributions for both the mineral platelets and the intercalated organic layers, the orientation distribution of the stacks, and an estimate for the average crystal size in the *c*-axis dimension. Furthermore, the equidistant meridional reflections originating from the periodicity of the density projection of the striated fibrils onto their axes due to the gap/overlap sequence were fitted simultaneously in 2D to the appropriate expressions, again by taking preferred orientation effects quantitatively into account (Burger *et al.*, 2007*a*). The 2D fitting approach of these non-trivial peak shapes, also taking a possible sample tilt into account (Fraser *et al.*, 1976), leads to more accurate and consistent values for the integrated intensities and for the long period. Additionally, it generates estimates for the lateral fibril size, longitudinal coherence lengths, and quantitative information about the orientation distribution function.

2. Experimental and data analysis

The samples used in this study were native intramuscular shad and herring bones. The system was chosen for its reduced structural hierarchy and simple fiber symmetry. The samples were prepared by paying special attention to preserve the native collagen/mineral superstructure as it was in the *in vivo* condition. SAXS experiments were carried out at the beamline X27C of the National Synchrotron Light Source (NSLS) at Brookhaven National Laboratory (BNL). In order to obtain high-quality SAXS patterns for the delicate quantitative analysis, a three pinhole collimation system was used to reduce the beam divergence (Chu & Hsiao, 2001) and a vacuum sample chamber was introduced to lower the background scattering from air and Kapton windows. In order to ensure the absence of systematic errors introduced by the detection system, two different types of detector technology (imaging plates and charge-coupled device) with different counting and readout mechanisms were used to record the scattering pattern from the same sampling volume, showing an

excellent agreement. Furthermore, it was found to be necessary to take the curvature of the Ewald sphere into account (as described by Fraser *et al.*, 1976), a correction that is normally neglected for SAXS (tangent plane approximation), but in the present case the overlap of the highest order meridional reflections with the Ewald sphere depend crucially on the latter's curvature and also on very small sample tilts which need to be taken into account as well. Other details about the sample preparation, instrumentation, image processing, and data analysis can be found in separate papers (Burger *et al.*, 2007*a*,*b*).

3. Results and discussion

Fig. 1 shows the hierarchical structures in the bone from human or other higher animals. The intramuscular shad/herring bones have a simplified hierarchy, in that they are directly built from collagen fibrils with their principal axes preferentially oriented about the primary bone axis. In other words, the entire intramuscular shad/herring bone can essentially be treated as a single collagen fiber, *i.e.*, a bundle of collagen fibrils. A typical SAXS pattern from herring bone is shown in Fig. 2 (left). The meridional reflections were analyzed by the scheme described in Burger *et al.* (2007*a*) and the 'butterfly' pattern was analyzed by the scheme described in Burger *et al.* (2007*b*). The calculated 2D pattern (Fig. 2, right) faithfully reproduced the features of the experimental pattern. The corresponding structural parameters extracted from the 2D fit are listed in Tables 1 and 2. The integrated intensities were strong for the 1st, 3rd, 5th order and weak for the 2nd, 4th orders, indicating a near-symmetric square-well density profile for the alternating gap/overlap arrangement along the fibril axis. The orientation distribution of the collagen fibrils with respect to the bone axis was found to be well described by the Onsager orientation distribution (Onsager, 1949). Hermans' orientation parameter P_2 was used to characterize the degree of preferred orientation, assuming simple fiber symmetry. The average fibril diameter could be estimated from the reciprocal of the lateral integral width of the meridional reflections after orientation effects had been removed, leading to a value of 54 ± 2 nm for the present herring bone sample. A longitudinal coherence length could be estimated from a constant intercept after extrapolating the longitudinal integral widths of the meridional reflections to zero order. It should be noted that the coherence lengths of the collagen fibrils determined in this work were different from those determined by Fraser *et al.* (1983). The former is related to the low-resolution features of molecular packing in the longitudinal direction, while the latter is related to the correlation of the gap/overlap sequence (Burger *et al.*, 2007*a*).

Table 1
Structural parameters obtained by fitting the meridional reflections in the measured SAXS diffraction pattern (Fig. 2, left).

Scaling is such that the 1st order is equal to 1000.

Order	Intensity
1	1000 (7)
2	52 (1)
3	405 (3)
4	16 (1)
5	138 (2)
6	83 (2)
7	20 (2)
9	38 (3)
11	32 (3)

Other parameters

Hermans' orientation parameter†	0.961 (1)
Average fibril diameter	54 (2) nm
Long period	66.4 (1) nm
Coherence length	0.94 (3) µm

† Referring to the orientation distribution of the collagen fibril axes with respect to the primary bone axis.

Table 2
Structural parameters obtained by fitting the measured 'butterfly' pattern (Fig. 2, left).

Hermans' orientation parameter is for the Onsager distribution (Burger *et al.*, 2007), $\langle T \rangle$ is the average thickness of mineral crystals, σ_T is the width of the thickness distribution of mineral crystals, $\langle t \rangle$ is the average thickness of organic collagen layers, σ_t is the width of the thickness distribution of organic layers, and H is average length of crystals in the c-axis dimension.

Hermans' orientation parameter†	$\langle T \rangle$ (nm)	σ_T (nm)	$\langle t \rangle$ (nm)	σ_t (nm)	H (nm)
0.883 (1)	2.05 (1)	0.05 (3)	5.47 (2)	3.09 (2)	51.2 (5)

† This is the orientation distribution of the long axes of the mineral crystals with respect to the primary bone axis.

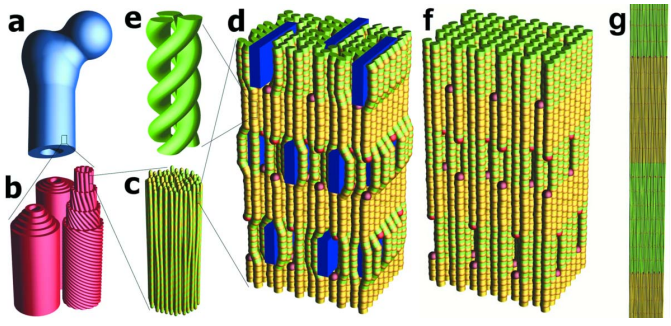

Figure 1
Schematic diagram of the hierarchical structures in bone from human or other higher animals. (a) Macroscopic bone: ~ a few cm. (b) Haversian osteons in cortical bone: ~100 µm, consisting of several concentric lamellar layers that are built from parallel collagen fibers. (c) Fine structure of collagen fiber: ~5 µm lateral, consisting of collagen fibrils: ~50–100 nm lateral. (d) Collagen molecular packing with mineral in the fibril: ~67 nm long period, ~1.5 nm lateral. Collagen molecules are shown as green and yellow rods. Mineral crystals are shown as blue tiles. The figure has a 10:1 aspect ratio distortion. (e) Single molecule triple helix: ~1.0 nm lateral. (f) Uncalcified collagen matrix (also with a 10:1 aspect ratio distortion). (g) True aspect ratio of molecular packing in fibril.

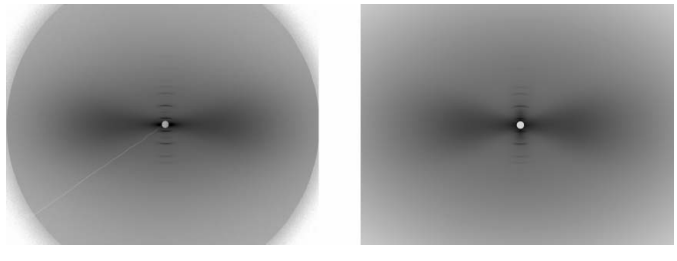

Figure 2
Measured pattern (left) *versus* calculated pattern (right) for SAXS from mineralized collagen fibrils of intramuscular herring bone. The bone axis is in the vertical direction, corresponding to the meridian of the present fiber symmetry. The equator is perpendicular to the bone axis. The calculated intensity on the right pattern is a combination of two components: (1) the sharp meridional reflections originating from the periodic packing of collagen molecules and mineral crystals along the fibril axis (Burger *et al.*, 2007*a*); and (2) the fan-shaped near-equatorial diffuse scattering originating from the lateral packing of mineral crystals in organic matrix (Burger *et al.*, 2007*b*). The fitting parameters for the calculated pattern are listed in Tables 1 and 2.

The parameters used to describe the lateral packing of the mineral crystals in the collagen matrix are listed in Table 2. The thickness of the mineral platelets is described by a Gaussian distribution and the thickness of the organic collagen layers between adjacent apatite platelets is described by a gamma distribution. It can be seen that the apatite platelets have a nearly uniform thickness ($\langle T \rangle \sim 2.05$ nm) with a narrow distribution ($\sigma_T \sim 0.05$ nm). On the other hand, the thickness of the organic layers have a broader distribution ($\sigma_t \sim 3.09$ nm) centered at $\langle t \rangle \sim 5.47$ nm. Such information is essential for the understanding of the 3D collagen/mineral superstructure on which the mechanical, physiological and biological functions of bone depend.

The authors thank Dr Dufei Fang for assistance with the X-ray diffraction analysis and Drs Lixia, Rong and Jinglu Chen for helping with the synchrotron X-ray experiments. We gratefully acknowledge support of this work by the National Institutes of Health (2 R01 AG014701-17A1) and the Department of Energy (DEFG0299ER45760) for operation of X27C at NSLS/BNL.

References

Burger, C., Zhou, H.-W., Sics, I., Hsiao, B. S., Chu, B., Graham, L. & Glimcher, M. J. (2007*a*). In preparation.
Burger, C., Zhou, H.-W., Sics, I., Hsiao, B. S., Chu, B., Graham, L. & Glimcher, M. J. (2007*b*). In preparation.
Chu, B. & Hsiao, B. S. (2001). *Chem. Rev.* **101**, 1727–1761.
Fraser, R. D. B., MacRae, T. P., Miller, A. &. Rowlands, J. (1976). *J. Appl. Cryst.* **9**, 81–94.
Fraser, R. D. B., MacRae, T. P., Miller, A. & Suzuki, E. (1983). *J. Mol. Biol.* **167**, 497–521.
Fratzl, P. (1994). *J. Stat. Phys.* **77**, 125–143.
Fratzl, P., Fratzl-Zelman, N. & Klaushofer, K. (1993). *Biophys. J.* **64**, 260–266.
Glimcher, M. J. (1998). *Metabolic Bone Disease and Clinically Related Disorders*, edited by L. V. Avioli and S. M. Krane, pp. 23–50. San Diego: Academic Press.
Hodge, A. J. & Petruska, J. A. (1963). *Aspects of Protein Structure*, edited by G. N. Ramachandran, pp. 289–300. New York: Academic Press.
Jackson, S. F. (1957). *Proc. R. Soc. London Ser. B*, **14**, 270–280.
Kim, H.-M., Rey, C. & Glimcher, M. J. (1995). *J. Bone Miner. Res.* **10**, 1589–1601.
Landis, W. J., Song, M. J., Leith, A., McEwen, L. & McEwen, B. F. (1993). *J. Struct. Biol.* **110**, 39–54.
Lee, D. D. & Glimcher, M. J. (1991). *J. Mol. Biol.* **217**, 487–501.
Onsager, L. (1949). *Ann. N Y Acad. Sci.* **51**, 627–659.
Robinson, R. A. (1952). *J. Bone Joint Surg.* **34**, 389–434.
Ruland, W. & Tompa, H. (1968). *Acta Cryst.* A**24**, 93–99.
Zernike, F. & Prins, J. A. (1927). *Z. Phys.* **41**, 184–194.